Hindawi
Advances in Polymer Technology
Volume 2023, Article ID 4986453, 13 pages
https://doi.org/10.1155/2023/4986453

*Research Article*

# Influence of Guluronic and Mannuronic Groups in Sodium Alginate Blends with Silk Fibroin: Phase Equilibrium and Thermodynamic Modeling

**Laise Maia Lopes** [1], **Mariana Agostini de Moraes** [2] **and Marisa Masumi Beppu** [1]

[1]*School of Chemical Engineering, State University of Campinas, Campinas, São Paulo, Brazil*
[2]*Department of Chemical Engineering, Institute of Environmental, Chemical and Pharmaceutical Sciences, Federal University of São Paulo, Diadema, São Paulo, Brazil*

Correspondence should be addressed to Laise Maia Lopes; mlopes.la@gmail.com

Received 17 September 2022; Revised 26 November 2022; Accepted 12 January 2023; Published 28 November 2023

Academic Editor: Vijay K. Thakur



Silk fibroin (SF) and sodium alginate (SA) are natural polymers with interesting properties to produce biomaterials. Blends of these polymers form a complex protein–polysaccharide system where phase separation can be observed. Therefore, the thermodynamic analysis of this system is important to understand the interaction between the polymers and predict the final state and composition of the phases found in these blends. This study explored blends with a different initial composition of SF, SA, and water at 25°C and neutral pH. The influence of the proportion between mannuronic and guluronic acids on SA composition was investigated. After phase separation, two phases were identified, and the equilibrium data were fitted on three different thermodynamic models: Flory–Huggins, non-random two-liquids, and universal quasichemical. Cohn equation was also used to investigate the potential of SA to precipitate the SF in solution. The results show that the proportion of mannuronic and guluronic acids on the SA can significantly influence on equilibrium data and on the SF/SA interaction parameter, hence, becoming a variability factor if this parameter is not under control in formulations.

## 1. Introduction

The systems formed by protein and polysaccharides are complex, and phase separation is often observed. Silk fibroin (SF, a fibrous protein extracted from silkworm cocoons [1]) and sodium alginate (SA, a polysaccharide extracted from brown algae [2–5]) blends have been studied over the years due to their intrinsic characteristics, such as biodegradability, biocompatibility, and low toxicity [6–9]. However, it forms a complex system where partial miscibility is observed [6, 10]. When in solution, phase separation is observed for SF–SA blends, and two phases are formed, one which is liquid and rich in SA and another which is solid-like, rich in SF, as shown in Figure S1 of the supplementary materials [10, 11].

The thermodynamic understanding of SF–SA interactions is important because their blends have been used extensively in tissue engineering, as dressing, scaffolds, and controlled release devices with a differentiated microstructure as a consequence of the interaction between the polymers [12–15]. The biocomposites of SF–SA also presented interesting mechanical properties, such as high flexibility and resistance to tear [15], due to the polymer interaction. Therefore, fundamental studies about the polymer interactions could stimulate the development of new products in this area. Moreover, the SA content of $\beta$-D mannuronic acid (M block) and $\alpha$-L guluronic acid (G block) seemed to influence the physicochemical, rheological, and mechanical properties of SA [16] and, consequently, could interfere on the properties of SF–SA blends. Therefore, it is extremely important to relate the thermodynamic properties of this system, to the influence of guluronic and mannuronic acids of SA, in order to fine-tune the characteristics of the blends, such as morphology, mechanical, and thermal properties.

The interaction between SF and SA occurs by intra and intermolecular hydrogen bonds [17, 18] between the hydroxyl/carboxyl and amine groups (Figure 1); however, the thermodynamic properties are not completely clear.

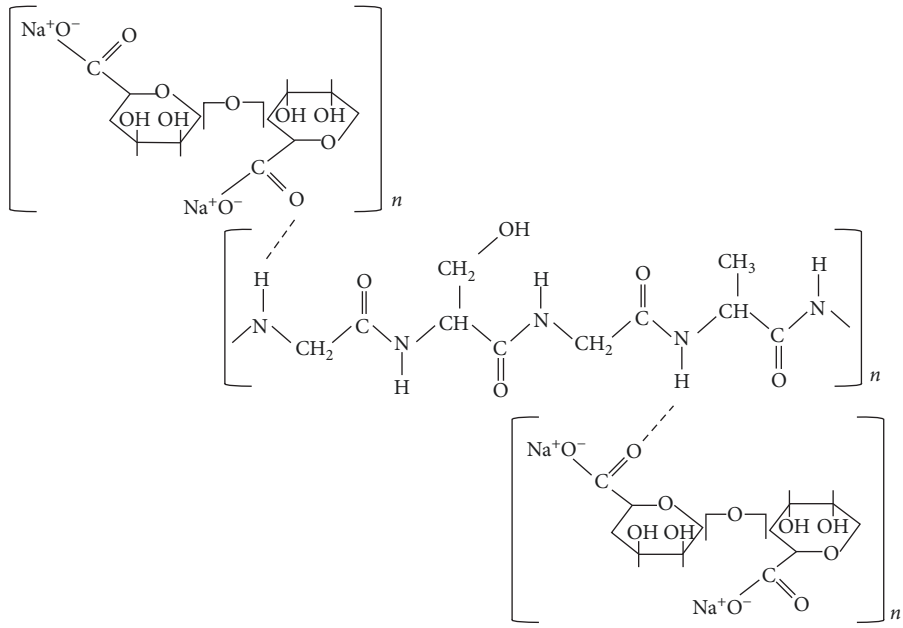

Figure 1: Illustration scheme of silk fibroin and sodium–alginate interaction.

Lopes et al. [19] studied SA and SF blends, observing that there is a small area in the phase diagram where the formation of two phases is observed and that SA, as other hydrophilic polymers, seems to interfere in the solvation of the SF in solution, having a salting-out effect [19, 20]. It is claimed that this effect probably accelerates the formation of $\beta$-sheet structures and the solid-like phase formation [10]. Therefore, fundamental studies, like the present one, are important to predict the system behavior and allow the blend production with specific properties.

In this study, equilibrium data of SF and SA blends were acquired and adjusted in three different thermodynamic models: Flory–Huggins, non-random two-liquids (NRTL), and universal quasichemical (UNIQUAC). The influence of the SA composition (proportion of M and G blocks) on the phase equilibrium and on the interaction parameters was investigated. Two alginates extracted from different seaweeds were used. Cohn equation was used to analyze the potential of SA to precipitate the SF and form the solid-like phase. Since the properties of the system can be directly influenced by blend composition, it is important to understand the parameters that can influence on the polymer interaction and consequently on blend miscibility.

## 2. Materials and Methods

*2.1. Natural Polymers.* The SF cocoons produced by *Bombyx mori* silkworm were donated by Bratac (Brazil). Two different SAs were used, both from FMC Polymers (USA), one extracted from *Macrocystis pyrifera* seaweed, which will be called alginate-M, and the other extracted from *Laminaria hyberboria* seaweed, which will be called alginate-G.

*2.2. Sodium Alginate Characterization*

*2.2.1. Determination of Viscosimetric Molar Mass.* The viscosimetric molar mass ($\overline{M_v}$) was estimated using the intrinsic viscosity data and the Mark–Houvink equation (Equation (1)).

$$\eta_{\text{int}} = K\left(\overline{M_v}\right)^{\alpha}, \tag{1}$$

where $K$ and $\alpha$ are constants equal to $1.228 \times 10^{-4}$ and 0.963, respectively, and $\eta_{\text{int}}$ is the intrinsic viscosity.

The intrinsic viscosity was measured by using SA solution with different concentrations (0.05, 0.10, 0.15, 0.20, 0.25, and 0.3 g/dL) diluted on 0.1 mol/L NaCl solution.

The tests were carried out using an Ostwald–Cannon–Fenske capillary viscometer and a thermostatic recirculation bath (Nova Ética, Brazil) at $25 \pm 0.1$°C. The volume of SA solution used was equal to 8.0 mL, and the flow time was marked with a digital stopwatch. For each solution, five time measurements were taken, and the average was used to calculate the viscosity. The relative ($\eta_{\text{rel}}$) and inherent ($\eta_{\text{ine}}$) viscosities were calculated using Equations (2) and (3), respectively, as follows:

$$\eta_{\text{rel}} = \frac{t}{t_0}, \tag{2}$$

$$\eta_{\text{ine}} = \frac{ln\eta_{\text{rel}}}{C}, \tag{3}$$

$$\eta_{\text{int}} = \lim_{C \to 0} \eta_{\text{ine}}, \tag{4}$$

where $t$ is the alginate solution flow time in the viscometer (s); $t_0$ is the pure solvent flow time in the viscometer (s); $C$ is the concentration of the alginate solution (g/dL).

*2.2.2. Determination of Mannuronic and Guluronic Acid Residues.* The molar ratio of $\beta$-D-mannuronic ($M$) and $\alpha$-L-guluronic ($G$) acid residues, the molar fractions of $GG$, $MM$, and $GM/MG$ and the sequences $F_{GG}$, $F_{MM}$, and $F_{(GM/MG)}$ were determined by $^1$H nuclear magnetic resonance ($^1$H-NMR) spectroscopy in deuterated water ($D_2O$) at 70°C using a Bruker

300 MHz spectrometer. The data obtained were analyzed using the MestReNova 14.1.0 software (Mestrelab Research S.L., Spain) and calculated using Equations (5)–(9) [21].

$$F_G = \frac{I_{5.05}}{(I_{4.67} + I_{4.45})}, \quad (5)$$

$$F_G + F_M = 1, \quad (6)$$

$$F_{GG} = \frac{I_{4.45}}{(I_{4.67} + I_{4.45})}, \quad (7)$$

$$F_G = F_{GG} + F_{GM}, \quad (8)$$

$$F_M = F_{MM} + F_{MG}, \quad (9)$$

where $I_{5.05}$, $I_{4.67}$, and $I_{4.45}$ are the peak intensities of 5.05, 4.67, and 4.45 ppm, respectively; $F_G$ is the molar fraction of the $G$ blocks; $F_M$ is the molar fraction of the $M$ blocks; $F_{GG}$, $F_{MG}$, $F_{MM}$, and $F_{GM}$ are the molar fractions of groups $GG$, $MG$, $MM$, and $GM$, respectively.

*2.3. SF and SA Solutions Preparation.* SF solution was prepared following the method previously published [6]. Briefly, silkworm cocoons were degummed using 1 g/L $Na_2CO_3$ solution in a thermostatic bath at 85°C (Nova Analitica, Brazil) for 30 min, and the process was repeated two times. The obtained fibers were washed with deionized water and maintained at room temperature until completely dry. They were milled and passed through a 10 mesh sieve and then solubilized in a ternary solution of $CaCl_2$ : ethanol : water (1 : 2 : 8 molar rate). To remove the salts, the solution was dialyzed using a membrane (MWCO 3.5 kDa, Thermo Fisher Scientific, EUA) and ultrapure water (1 : 10 rate). To remove the insoluble parts that are formed during dialysis, the solution was centrifuged for 30 min and 2,300 relative centrifugal force.

SA powder extracted from *M. pyrifera* and *Laminaria hyperboria* was dissolved in deionized water with a concentration of 2% (w/v). The solution was kept for 3 days, so the water could solvate the powder, and then the solution was homogenized by stirring. To perform the SA quantification, it was necessary to label it with 4,6 diamidino-2-phenylindole (DAPI). First, 1-ethyl-3 (3-dimethylaminopropyl) carbodiimide (EDC) (0.2 mg/mL) was added to the SA solution under stirring at 4°C. After EDC dissolution, DAPI was added in a concentration equal to 0.1 mg/mL. The alginate-DAPI system was kept in an ice bath and under agitation for 48 hr. The resulting solution was dialyzed for 72 hr using 1 : 100 distilled water, changed every 24 hr.

*2.4. Blend Preparation.* To prepare the SF/SA blends, SF solution was added to the SA solution slowly and under magnetic stirring in different mass proportions. There was no pH adjustment after the preparation of the solutions, which were around 7.0 for both polymeric solutions. The mass proportions that were used were based on previous work [10] and are shown in Table 1. The blends were kept at room temperature, around 25°C, in a thermostatic bath (Tecnal, Brazil). The nomenclature used in the work to refer to the blends of SF and SA will be SF$x$SA$y$WA$z$, where $x$, $y$, and $z$ are the mass fractions of the components (in percentage), SF is silk fibroin, SA is sodium alginate, and WA is water.

Table 1: Initial mass fraction ($w$) of silk fibroin (SF), sodium alginate (SA), and water (WA) blends.

| Blend | WSF | WSA | WWA |
|---|---|---|---|
| $SF_{0.5}SA_{0.5}WA_{99}$ | 0.005 | 0.005 | 0.990 |
| $SF_{1.0}SA_{0.5}WA_{98.5}$ | 0.010 | 0.005 | 0.985 |
| $SF_{1.5}SA_{0.5}WA_{98}$ | 0.015 | 0.005 | 0.980 |
| $SF_{0.5}SA_{1.0}WA_{98.5}$ | 0.005 | 0.010 | 0.985 |
| SF1,0SA1,0$WA_{98}$ | 0.010 | 0.010 | 0.980 |
| $SF_{1.5}SA_{1.0}WA_{97.5}$ | 0.015 | 0.010 | 0.975 |
| $SF_{0.5}SA_{1.5}WA_{98}$ | 0.005 | 0.015 | 0.980 |
| $SF_{1.0}SA_{1.5}WA_{97.5}$ | 0.010 | 0.015 | 0.975 |
| $SF_{1.5}SA_{1.5}WA_{97}$ | 0.015 | 0.015 | 0.970 |
| $SF_{0.5}SA_{2.0}WA_{97.5}$ | 0.005 | 0.020 | 0.975 |
| $SF_{1.0}SA_{2.0}WA_{97}$ | 0.010 | 0.020 | 0.970 |
| $SF_{0.5}SA_{2.5}WA_{97}$ | 0.005 | 0.025 | 0.970 |

*2.5. Optical and Fluorescence Microscopy.* The optical microscopy was used to analyze the morphology of the mixture between SF solution and SA after mixing the two solutions. For this, the SA solution was placed on a glass slide; then, the SF solution was added to the SA solution and gently mixed with a spatula. Nikon optical microscope (Tokyo, Japan) model Eclipse E200 was used to take images of the blend.

The fluorescence microscopy was used to investigate the composition of the globular structures observed after blend formation. The SA labeled with DAPI, as described before, was used, and the blends were analyzed with a Zeiss model LSM 710 fluorescence microscope (Germany).

*2.6. Components Phase Quantification.* The amount of water was quantified by evaporation in both phases. To perform the quantification of SA in the liquid phase, it was necessary to label it with a fluorescent molecule, DAPI, as described before. After labeling it, the alginate was quantified by fluorescence spectroscopy in a Varioskan LUX Plate Reader (ThermoFisher Scientific, USA) at 358 nm (emission) and 461 nm (excitement).

SF was quantified, in liquid phase, by Bradford's method of protein quantification. This method was chosen because it does not suffer interference from polysaccharides. The standard curve was prepared using SF solution instead of bovine serum albumin to obtain more reliable results. The analysis was performed using 96-well plates, in which 10 $\mu$L of the sample was mixed with 190 $\mu$L of Bradford reagent (Scienco, Brazil). After 30 min, the plate was read at 595 nm in a Varioskan LUX Plate Reader (ThermoFisher Scientific, USA).

Table 2: Density and specific volume values of sodium alginate, silk fibroin, and water used to calculate the Flory–Huggins parameters.

| | Density (g/cm³) | Specific volume (cm³/g) | Reference |
|---|---|---|---|
| Water | 1.00 | 1.00 | |
| Sodium alginate | 0.875 | 1.14 | [22] |
| Silk fibroin | 1.32 | 0.757 | [23] |

In the solid phase, both SF and SA were quantified by mass balance, using Equation (10).

$$m_i^{SP} = m_i^T - m_i^{LP}, \tag{10}$$

where $m_i^T$, $m_i^{SP}$, and $m_i^{LP}$ are the total blend mass, the mass of the component in the solid phase and the mass of the component in the liquid phase, respectively.

## 3. Thermodynamic Model Calculation

*3.1. Flory–Huggins Modeling.* Equation (11) was used to estimate Flory–Huggins parameters. For each component, in each phase, Equation (11) can be written as shown in Equations (12)–(14), obtaining a linear equations system, which can be easily solved.

$$\ln a_i = 1 + \ln \varphi_i - V_i \sum_i \frac{\varphi_i}{V_i} + \frac{V_i}{V_s}\left(\sum_j \frac{\chi_{ij}}{T}\varphi_j - \sum_k \sum_{j>k} \frac{\chi_{kj}}{T}\varphi_k\varphi_j\right), \tag{11}$$

where $a_i$ is the activity, $\varphi_i$, $\varphi_j$, and $\varphi_k$ are the volumes fractions of component $i$, $j$, and $k$, $V_i$ is the volume of component $i$, $V_s$ is the volume of the solvent, $T$ is the temperature, $\chi_{ij}$ is the interaction parameter of $i$ and $j$ components, and $\chi_{kj}$ is the interaction parameter of $k$ and $j$ components.

$$\begin{aligned}\ln a_{\mathrm{SF}} = {} & \ln \varphi_{\mathrm{SF}} + (1 - \varphi_{\mathrm{SF}}) - \left(\frac{V_{\mathrm{SF}}}{V_{\mathrm{SA}}}\right)\varphi_{\mathrm{SA}} - \left(\frac{V_{\mathrm{SF}}}{V_{\mathrm{WA}}}\right)\varphi_{\mathrm{WA}} \\ & + ((\chi_{\mathrm{SASF}}\varphi_{\mathrm{SA}} + \chi_{\mathrm{SFWA}}\varphi_{\mathrm{WA}}) * (\varphi_{\mathrm{SA}} + \varphi_{\mathrm{WA}})) \\ & - \chi_{\mathrm{SAWA}}\left(\frac{V_{SF}}{V_{\mathrm{SA}}}\right)\varphi_{\mathrm{SA}}\varphi_{\mathrm{WA}},\end{aligned} \tag{12}$$

$$\begin{aligned}\ln a_{\mathrm{SA}} = {} & \ln \varphi_{\mathrm{SA}} + (1 - \varphi_{\mathrm{SA}}) - \left(\frac{V_{\mathrm{SA}}}{V_{\mathrm{SF}}}\right)\varphi_{\mathrm{SF}} - \left(\frac{V_{\mathrm{SA}}}{V_{\mathrm{WA}}}\right)\varphi_{\mathrm{WA}} \\ & + \left(\left(\chi_{\mathrm{SASF}}\varphi_{\mathrm{SF}}\frac{V_{\mathrm{SA}}}{V_{\mathrm{SF}}} + \chi_{\mathrm{SAWA}}\varphi_{\mathrm{WA}}\right) \times (\varphi_{\mathrm{SF}} + \varphi_{\mathrm{WA}})\right) \\ & - \chi_{\mathrm{SFWA}}\left(\frac{V_{\mathrm{SA}}}{V_{\mathrm{SF}}}\right)\varphi_{\mathrm{SF}}\varphi_{\mathrm{WA}},\end{aligned} \tag{13}$$

Table 3: Area ($r$) and volume ($q$) parameter values calculated from Equations (17) and (18) for silk fibroin, sodium alginate, and water.

| Substance | $r$ | $q$ |
|---|---|---|
| Sodium alginate | 6.0192 | 5.301 |
| Silk fibroin | 10.1413 | 9.415 |
| Water | 0.9200 | 1.400 |

$$\begin{aligned}\ln a_{\mathrm{WA}} = {} & \ln \varphi_{\mathrm{WA}} + (1 - \varphi_{\mathrm{WA}}) - \left(\frac{V_{\mathrm{wA}}}{V_{\mathrm{SF}}}\right)\varphi_{\mathrm{SF}} - \left(\frac{V_{\mathrm{WA}}}{V_{\mathrm{SA}}}\right)\varphi_{\mathrm{SA}} \\ & + \left(\left(\chi_{\mathrm{SFWA}}\varphi_{\mathrm{SF}}\frac{V_{\mathrm{WA}}}{V_{\mathrm{SF}}} + \chi_{\mathrm{SAWA}}\varphi_{\mathrm{SA}}\right) \times (\varphi_{\mathrm{SF}} + \varphi_{\mathrm{SA}})\right) \\ & - \chi_{\mathrm{SFSA}}\left(\frac{V_{\mathrm{WA}}}{V_{\mathrm{SF}}}\right)\varphi_{\mathrm{SF}}\varphi_{\mathrm{SA}}.\end{aligned} \tag{14}$$

The volume fraction was calculated from the mass fraction using Equation (15). The density and specific volume values for SA [22], SF [23], and water are shown in Table 2.

$$\varphi_i = \frac{\frac{w_i}{p_i}}{\sum \frac{w_i}{p_i}}. \tag{15}$$

*3.2. NRTL and UNIQUAC Models.* The modeling of experimental data for the NRTL and UNIQUAC models was performed using the TME-LLE version 2.0 software written in Fortran language [24]. The software was developed to estimate the binary interaction parameters for Gibbs free energy models with any number of components and different temperatures through the minimization of the objective function (FO) shown in Equation (16) using the modified simplex method.

$$\mathrm{FO} = \sum_j^N \sum_i^P \left(x_{i,N}^{LP,\mathrm{exp}} - x_{i,N}^{LP,\mathrm{cal}}\right)^2 + \left(x_{i,N}^{SP,\mathrm{exp}} - x_{i,N}^{SP,\mathrm{cal}}\right)^2, \tag{16}$$

where $n$ is the number of tie lines of each system, $P$ is the number of components, $x_{i,N}^{LP,\mathrm{exp}}$ and $x_{i,N}^{LP,\mathrm{cal}}$ are the experimental and calculated molar fraction of component $i$ in the liquid phase, respectively, and $x_{i,N}^{SP,\mathrm{exp}}$ and $x_{i,N}^{SP,\mathrm{cal}}$ are experimental and calculated molar fraction of component $i$ in the solid phase, respectively.

The $r$ and $q$ structure parameters used in the UNIQUAC model were estimated using the subgroup contribution method, according to Equations (17) and (18), and are shown in Table 3. The parameter values of $R_k$ and $Q_k$ were taken from the literature [25]. This was necessary, as there is no information in the literature about the $r$ and $q$ parameters for SA and SF. For fibroin, the subgroups considered were those present in the chemical structure of alanine, serine, and glycine, which are the main amino acids present in the structure of SF. As for SA, the subgroups of $\alpha$-L-guluronic acid and $\beta$-D-mannuronic acid were considered.

$$r_i = \sum_k \vartheta_k^i R_k, \tag{17}$$

$$q_i = \sum_k \vartheta_k^i Q_k, \tag{18}$$

where $\vartheta_k^i$ is the numbers of $k$ type subgroups in a molecule $i$, $R_k$ and $Q_k$ are the relative volume and the relative area of each subgroup in the molecule, respectively.

The root mean square deviation (RMSD) was used to evaluate the correlation between experimental and theoretical data obtained by the thermodynamical models, and it is shown in Equation (19).

$$\mathrm{RMSD} = \sqrt{\frac{\sum_{1}^{N}\sum_{i=1}^{P}\left\{\left(w_{i,n}^{LP,\mathrm{exp}} - w_{i,n}^{LP,\mathrm{cal}}\right)^2 + \left(w_{i,n}^{SP,\mathrm{exp}} - w_{i,n}^{SP,\mathrm{cal}}\right)^2\right\}}{2NP}}, \tag{19}$$

where $n$ is the number of tie lines of each system, $P$ is the number of components, and the exp and cal refer to the calculated and experimental values of mass fraction, respectively.

*3.3. Cohn Equation.* For protein systems with or without electrolytes that present liquid–solid separation with the formation of precipitates, such as the fibroin-alginate blend, a simple equation that adjusts the equilibrium data is the Cohn [26] equation, that relates the protein solubility with the salting-out constant ($K_s$).

The study of SF solubility in different SA solutions was carried out using samples with constant volume of silk solutions with different concentrations of SA solutions. Samples containing 4.5 mL of SA solution and 0.5 mL of 2% SF solution were prepared. The concentration of SA solutions varied from 0.4% to 1.4% (m/m). The blends were kept in a thermostatic bath at 25°C for 8 days. The phases were separated by centrifugation, and the polymers were quantified in the liquid phase as previously described. After quantification, the data were adapted to the Cohn equation (Equation (20)) and the solubility constants $\beta$ ($K_s$) were determined.

$$\ln(S) = \beta - K_s m, \tag{20}$$

where $S$ is the solubility of the protein, $K_s$ is the protein solubility constant, $m$ is the concentration of the precipitating agent, and $\beta$ is the constant related to the net charge of the protein; for nonelectrolytes, this parameter is related to the solubility of the protein in the absence of precipitating agents.

Table 4: Values of intrinsic viscosity and viscosimetric molar mass for alginate-M and alginate-G.

| | Alginate-M | Alginate-G |
|---|---|---|
| $\eta_{\mathrm{int}}$(dL/g) | 4.47 | 8.21 |
| $\overline{M_v}$(Da) | $5.45 \times 10^4$ | $1.02 \times 10^5$ |
| $M/G$ | 2.03 | 0.43 |
| $F_M$ | 0.67 | 0.30 |
| $F_G$ | 0.33 | 0.70 |
| $F_{MM}$ | 0 | 0.14 |
| $F_{GG}$ | 0.33 | 0.54 |
| $F_{MG,GM}$ | 0.67 | 0.16 |

Proportion between $M$ and $G$ blocks, molar fraction of $M$ blocks ($F_M$), $G$ blocks $G$ ($F_G$), $GG$ blocks ($F_{GG}$), $MM$ blocks ($F_{MM}$), and $MG$/$GM$ blocks ($F_{MG,GM}$) for alginate-M and alginate-G.

Table 5: Values of Flory–Huggins parameter of interaction for the system silk fibroin–sodium alginate–water calculated with the equilibrium data at 25°C.

| | $X_{\mathrm{SASF}}$ | $X_{\mathrm{SFWA}}$ | $X_{\mathrm{SAWA}}$ | RMSD |
|---|---|---|---|---|
| Alginate-M | 0.0087 | 0.1240 | 0.0301 | 1.93 |
| Alginate-G | 0.0060 | 0.0886 | 0.0163 | 1.41 |

## 4. Results and Discussion

*4.1. Sodium Alginate Characterization.* The results of viscosity and viscosimetric molar mass for alginate-M and alginate-G are shown in Table 4. The viscosity and molar mass of the alginates are significantly different; the alginate extracted from *L. hyberboria* seaweed has a higher viscosity and molar mass than the alginate extracted from *M. pyrifera* seaweed.

The hydrogen NMR spectra ($^1$H-NMR) for the two types of alginate used are shown in Figure S2 of the supplementary materials. The spectra showed characteristic signals between 5.05 and 4.55 ppm, referring to the hydrogen bond of the G and M blocks, respectively [21, 27]. The fractions of the M and G blocks and their proportion for the studied alginates are shown in Table 5. The spectra of alginates showed chemical shifts close to 5.3 ppm, which can be attributed to the reducing end hydrogen [27], which is found in higher values when compared to the hydrogen in the inner chain. The presence of this sign suggests alginates with lower molar mass [21].

The ratio between M and G blocks reported in the literature for SAs extracted from brown seaweed is between 0.4 and 1.94, being higher in SAs from *M. pyrifera* seaweed [28, 29]. The amount of G and M blocks present in the polymer chain is directly related to its configuration and, consequently, to its interaction with other polymers and ions. As shown in Table 4, alginate-M, extracted from *M. pyrpyrifera*, has a higher proportion of mannuronic groups (M)

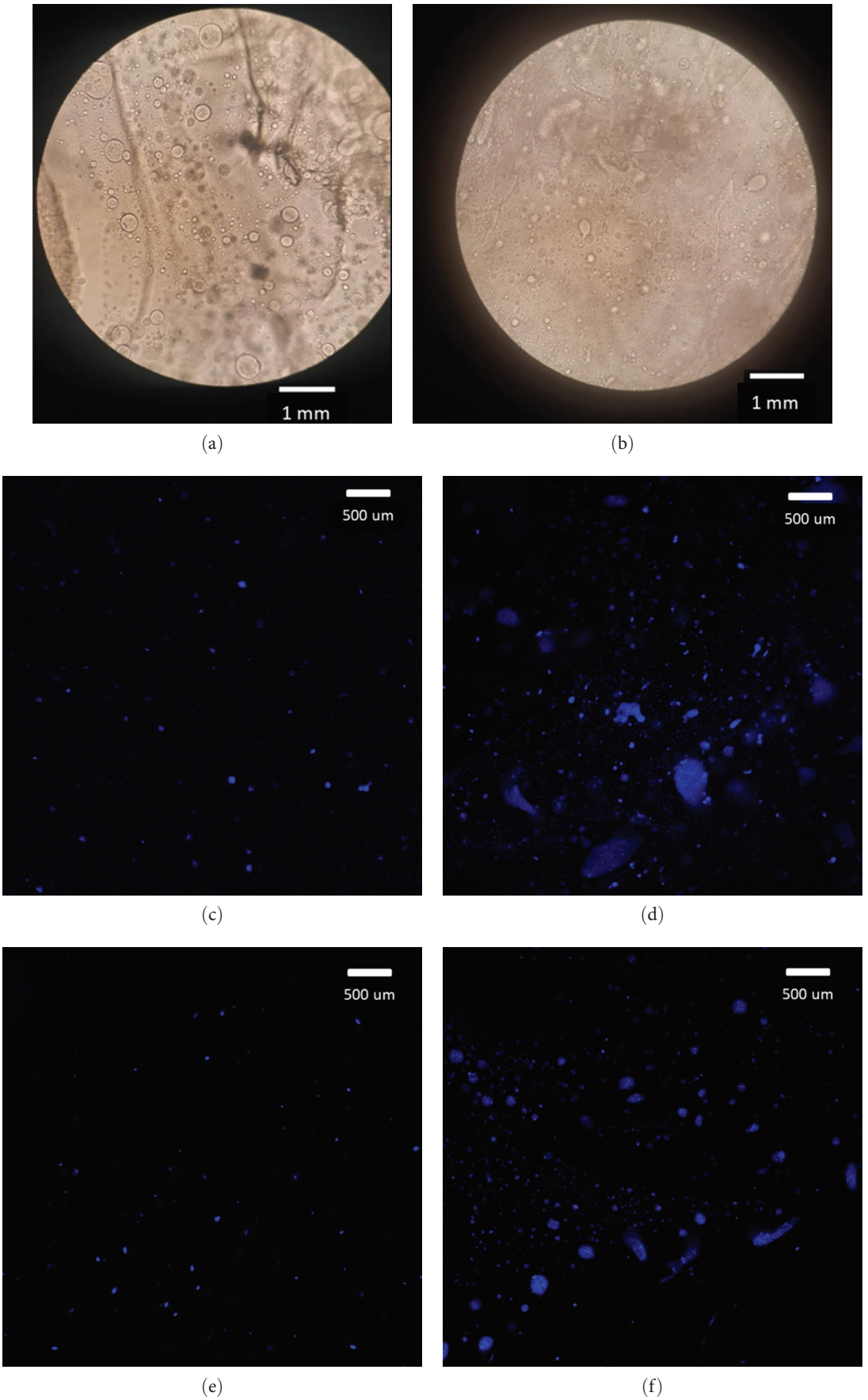


(a) (b) (c) (d) (e) (f)

FIGURE 2: Image of optical microscopy obtained immediately after the blend preparation ($SF_{0.5}SA_{0.5}WA_{98}$) with alginate-M (a) and alginate-G (b). Images obtained with fluorescence microscopy for alginate-M (c) and alginate-G (d) solutions, silk fibroin and sodium alginate blends ($SF_{0.5}SA_{0.5}WA_{98}$) with alginate-M (e) and alginate-G (f).

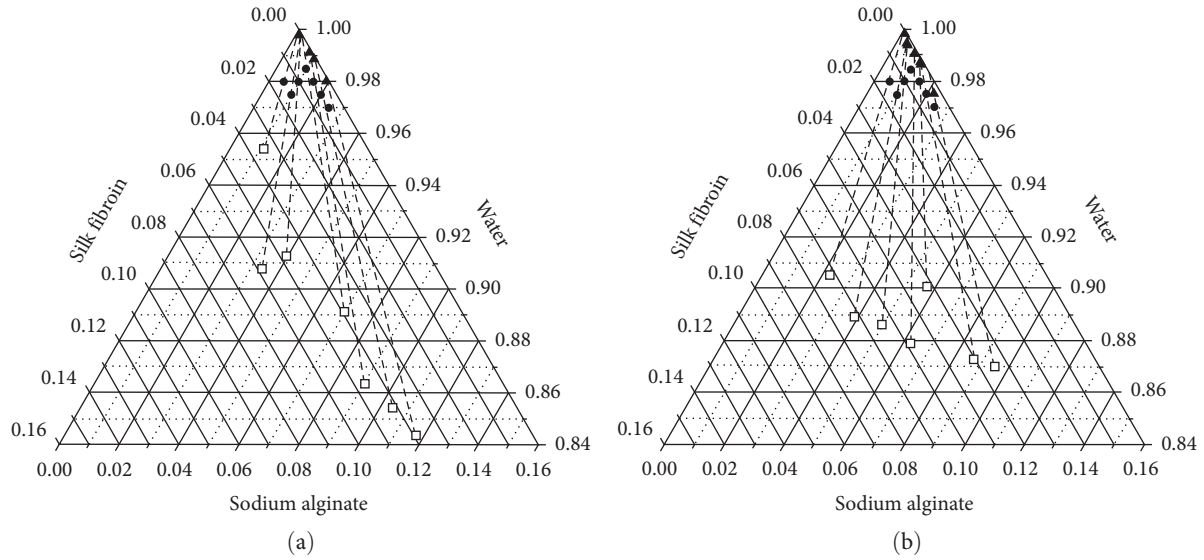


Figure 3: Phase diagram for blends of silk fibroin and alginate-M (a) and silk fibroin and alginate-G (b). Liquid phase (▲), solid phase (□), initial mixture points (●), and tie lines (- -).

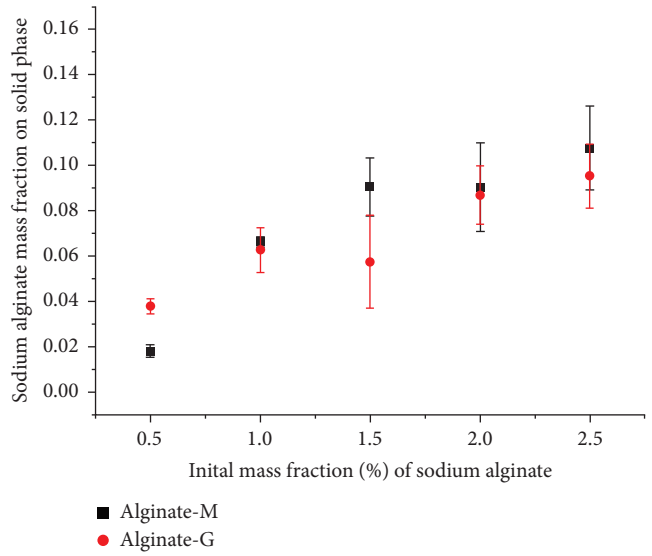


Figure 4: Alginate-M and alginate-G mass fraction on solid phase after phase separation as a function of the sodium alginate initial mass fraction on the blends with 0.5% of silk fibroin mass fraction.

in the chain, which are predominantly alternated (MG/GM), while alginate-G, extracted from *Laminaria hyperborea*, has a higher proportion of guluronic groups (G and GG).

*4.2. Optical and Fluorescence Microscopy.* Figure 2 shows the optical microscopy image obtained after mixing the SA and SF solutions. It is observed the formation of micelle-like structures, with a mean diameter of $0.247 \pm 0.120$ mm, indicating that phase separation occurs immediately after the polymers mixing. During the preparation of the SF and SA blends, it is possible to notice that when SF solution is added to SA solution, the blend becomes cloudy, with a milk-like aspect. The turbidity could be associated with the formation of these structures, which could interact and coalesce over time, trapping water molecules and forming a solid-like phase observed after some days in these blends, as described in previous work [10].

The fluorescence microscopy was performed to investigate the composition of these micelle-like structures. The alginate-M and alginate-G were labeled with DAPI as described previously; the images obtained are shown in Figure 2. It is possible to observe the SA particles labeled with DAPI before the addition of fibroin, as they show homogeneous fluorescence. After the addition of fibroin, the same micelle-like structures observed with the optical microscope were detected with the fluorescence microscope. It can be seen that they contain SA but are heterogeneous, indicating the presence of SF. It is possible to observe SA outside the structures, indicating that part of the polymer remains in the second phase. Similar structures were

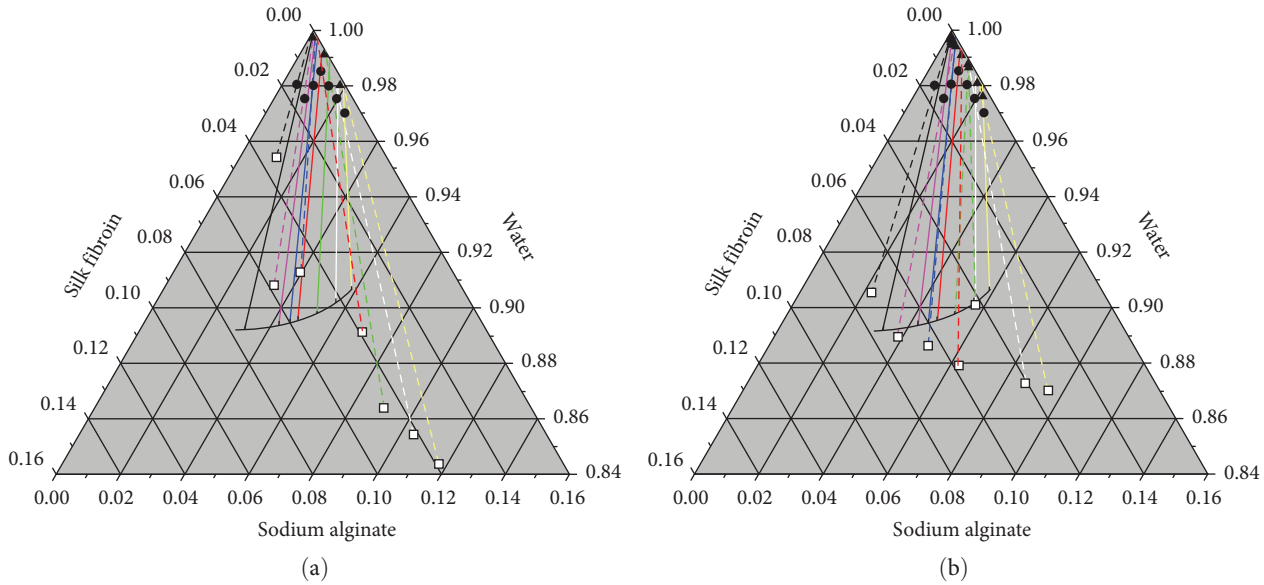


Figure 5: Phase diagram for blends of silk fibroin, water, and alginate-M (a) and silk fibroin, water, and alginate-G (b) at 25°C. Initials points of mixture (●), liquid phase (▲), solid phase (□). Tie lines obtained with experimental data (-.-) and obtained with Flory–Huggins model (-).

Table 6: Values of interaction parameters and RMSD for the systems composed by silk fibroin (1), sodium alginate (2), and water (3) for NRTL and UNIQUAC models for different sodium alginate.

| Model | System | $i,j$ | $A_{i,j}$ | $A_{j,i}$ | $\alpha_{i,j}$ | RMSD |
|---|---|---|---|---|---|---|
| NRTL | Alginate-M | 1,2 | −3000.0 | −2665.4 | 0.3760 | 1.07 |
| | | 1,3 | −1925.8 | 10,392 | 0.2000 | |
| | | 2,3 | 782.10 | 2971.2 | 0.4700 | |
| | Alginate-G | 1,2 | 935.01 | −65.914 | 0.4700 | 0.99 |
| | | 1,3 | −2520.3 | 15,031 | 0.2000 | |
| | | 2,3 | 2183.4 | −15.325 | 0.2598 | |
| UNIQUAC | Alginate-M | 1,2 | 8636.1 | −332.16 | – | 0.56 |
| | | 1,3 | −553.24 | 990.73 | – | |
| | | 2,3 | −163.24 | 548.37 | – | |
| | Alginate-G | 1,2 | 809.31 | −265.50 | – | 0.45 |
| | | 1,3 | −519.67 | 1052.9 | – | |
| | | 2,3 | −109.94 | 342.78 | – | |

observed in SF and SA membranes [6, 11]. De Moraes et al. [6] found that the structures observed were formed by both polymers and that after the formation of the membrane, it is possible to extract the SF and obtain porous membranes, providing a very interesting microstructure for this material. So, it is possible that the globules observed in the membranes are formed during the blend preparation. The formation of micelle-like structures has also been observed in other polysaccharide and protein systems, such as alginate-casein and alginate-soy protein [30, 31].

*4.3. Phase Equilibrium.* After 8 days of the blend preparation, two distinct phases are observed, one liquid and another solid-like, as described in previous work [10]. The quantification was carried out after reaching thermodynamic equilibrium, that is, on the 8 days after the preparation of the blend [11]. The mass fraction values of SF, SA, and water in each phase are shown in Table S1 of supplementary materials, and the ternary diagrams for the blends prepared with the different SAs are shown in Figure 3.

After the phase separation, SA is expected to remain in the liquid phase, as it is a hydrophilic polymer and has greater affinity with the water. However, blends with a higher mass fraction of SA also presented a greater amount of this polymer in the solid phase. The analysis was performed by comparing blends with the same initial mass fraction of SF and different mass fractions of SA, as shown in Figure 4. It is possible that the micelles-like structures formed after the preparation of the blends agglomerate and precipitate, forming the solid-like phase. Thus, one hypothesis is that blends with a higher initial mass fraction of SA form micelles with a higher concentration of this polymer, trapping it and enriching the solid phase. This behavior was observed by other authors for the fibroin-alginate system and for other

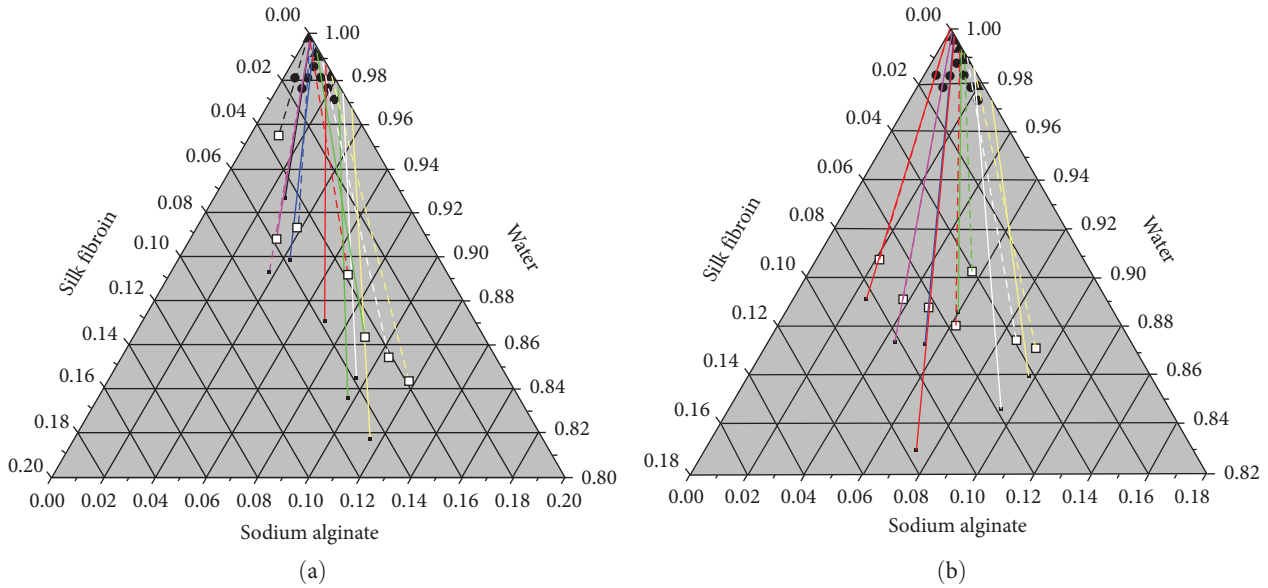


Figure 6: Phase diagram for blends of silk fibroin, water, and alginate-M (a) and silk fibroin, water, and alginate-G (b) at 25°C. Initials points of mixture (●), liquid phase (▲), solid phase (□). Tie lines obtained with experimental data (-.-) and obtained with NRTL model (-).

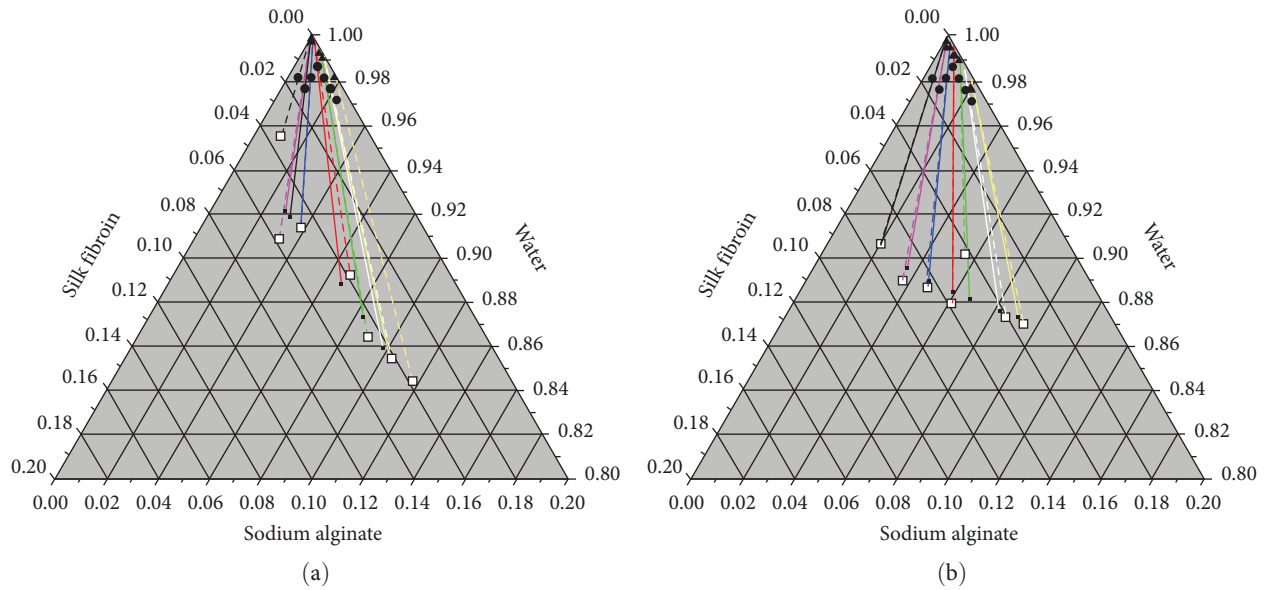


Figure 7: Phase diagram for blends of silk fibroin, water, and alginate-M (a) and silk fibroin, water, and alginate-G (b) at 25°C. Initials points of mixture (●), liquid phase (▲), solid phase (□). Tie lines obtained with experimental data (-.-) and obtained with UNIQUAC model (-).

protein–polysaccharide systems such as alginate-pea protein and $\kappa$-carrageenan-soy protein [31–33].

### 4.4. Thermodynamic Model Fitting

*4.4.1. Flory–Huggins.* The values of the Flory–Huggins parameters are shown in Table 5, and the calculated mass fraction values from the model are shown in Tables S2 and S3 in supplementary materials, which have been plotted in the ternary diagrams shown in Figure 5. In Figure 5, each point was represented by a color to facilitate the reader's visualization and interpretation. Fibroin–alginate interaction parameter values ($\chi_{SFSA}$) were close to those found in previous works in which glass transition temperature data were used to calculate them [10]. The values of $\chi_{SAWA}$ and $\chi_{SFWA}$ varied in relation to the type of SA used but remained in the same order of magnitude. The parameters were adjusted from the experimental data, and since they are different for systems with different types of alginates, it is expected that the values will vary a little. For SA, the value of the alginate–water interaction parameter reported in the literature is around 0.025 [34], and for SF, this value is close to 0.95 [35].

The binodal curve can be experimentally determined by the cloud point method, in which the clear solutions of the polymers are mixed in a controlled method until the blend

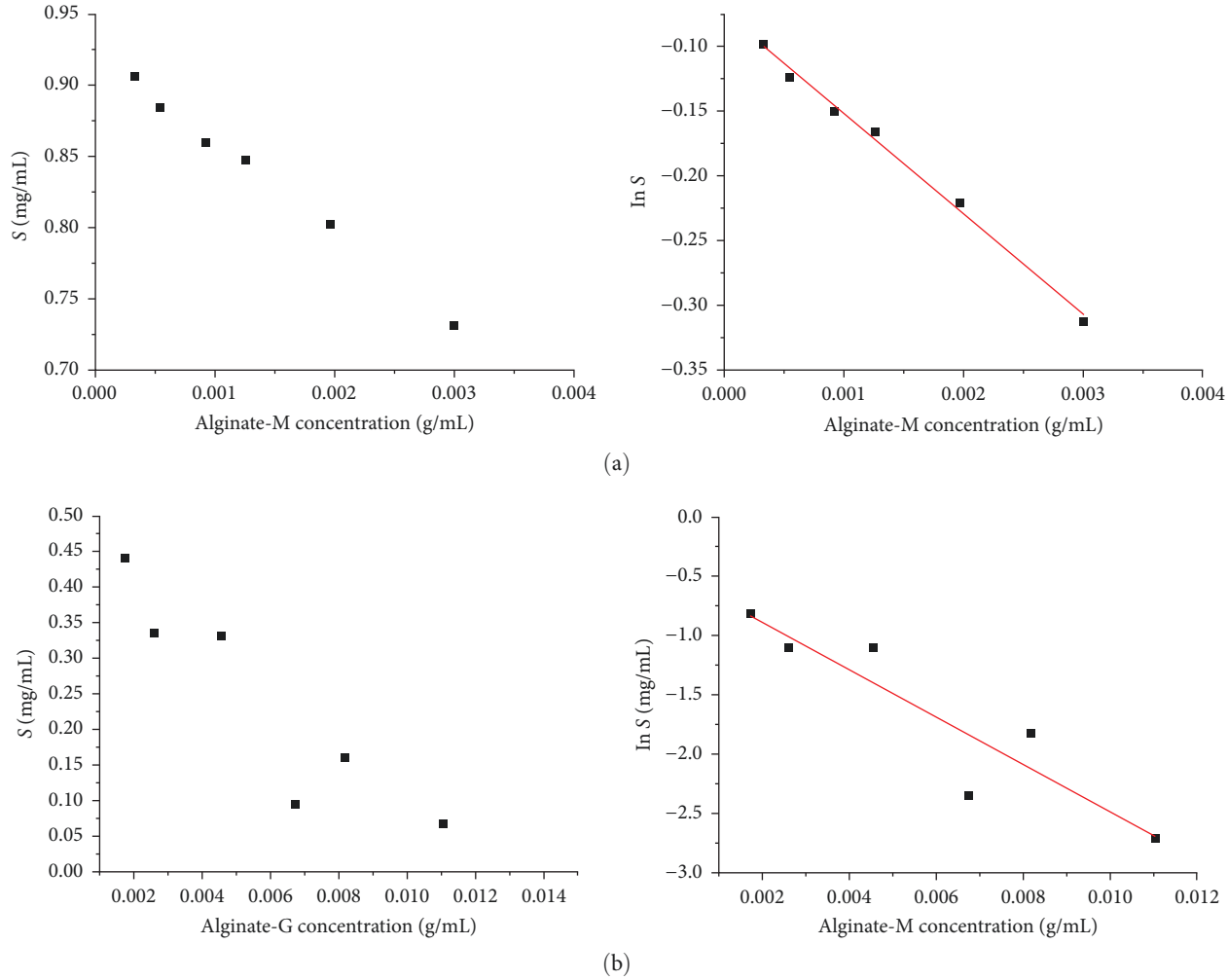


FIGURE 8: Solubility of silk fibroin in alginate-M (a) and alginate-G (b) at 25°C (1). Linearization of experimental data to obtain the parameters of Cohn equation (2).

becomes cloudy, and the mixture is considered two-phase. For the fibroin–alginate system, this experiment is difficult to carry out in practice due to the micelles-like formation and the rapid turbidity of the blend, even in low mass fractions of SF and SA. However, it was possible to estimate the binodal curve from the Flory–Huggins model, shown in Figure 5. The RMSD value of the model was about 2%. Despite the values are small, the poor adequacy of the experimental data to the Flory–Huggins model is easily noticed in the ternary diagram. As it is a small region of the phase diagram, small variations in the mass fraction can cause significant changes in the diagram's tie lines.

*4.4.2. NRTL and UNIQUAC Models.* The experimental data of mass fraction were also used to calculate the interaction parameters of the NRTL and UNIQUAC models, shown in Table 6. The mass fraction values calculated from the thermodynamic models are shown in Tables S4–S7 in supplementary materials and were plotted in the ternary diagrams shown in Figures 6 and 7. For the NRTL model, the values of the adjustable ($A_{i,j}$ and $A_{j,i}$) and nonrandom ($\alpha_{i,j}$) fibroin–alginate and alginate–water parameters presented significantly different values when changing the type of SA used in the blend. The same was not observed for the adjustable parameters related to the fibroin–water pair, which have different values but of the same order of magnitude.

The UNIQUAC model presented a good fit to the experimental data, shown in Figure 7. Unlike the NRTL model, the adjustable parameters ($A_{i,j}$ and $A_{j,i}$) did not show significant differences with the change in the type of SA. The values had the same order of magnitude for both systems, except for the parameter $A_{1,2}$, referring to the fibroin-alginate adjustable parameter. The differences between the observed parameters may be a consequence of the change in the configuration of the SA chain, since no significant changes were observed for the fibroin–water pair. The fraction of groups M and G in the SA chain causes a change in the arrangement of the functional groups. However, it is important to recognize that the molar mass can have an effect on the entropy of the mixture, since the greater its value, the greater the polymer chain and the smaller the possibilities of molecular arrangement. These two factors (disposition of M/G blocks and molar mass) can cause changes in the interaction between SA and the other components. The NRTL and UNIQUAC models had lower

Table 7: Constant of solubility ($K_s$) and constant $\beta$ obtained by the linearization of Cohn equation.

| | $\beta$ | $K_s$ (mL/g) | $R^2$ |
|---|---|---|---|
| Alginate-M | −0.0746 | 77.4 | 0.99 |
| Algnate-G | −0.4936 | 199.3 | 0.85 |

RMSD values than the Flory–Huggins model, and the one that best suited the experimental data was the UNIQUAC. This may happen because the UNIQUAC model uses the shape and volume data of the molecules involved in the system to determine the adjustable parameters, which can generate better results.

*4.4.3. Cohn Equation.* Another thermodynamic approach for the system is based on the study of the salting-out effect of SA in the ternary system, which was investigated by the Cohn equation, which can be used to analyze liquid–solid phase separations. The parameters $\beta$ and $K_s$ obtained from the adjustment of the experimental data (Figure 8) for each system are shown in Table 7. The parameter $K_s$ is called the salting out constant and expresses the ability of SA to induce this effect. The value obtained for alginate-G was higher than alginate-M, which suggests that it has a greater capacity to precipitate SF.

The salting-out phenomenon occurs when water-soluble molecules are excluded from the aqueous phase due to the high concentration of salt [36]. Despite not being, by definition, a salt, SA promotes a similar effect. Due to its hydrophilicity, the polymer remains solvated in water, stimulating fibroin–fibroin interactions and its subsequent precipitation. A similar phenomenon is observed in fibroin-PEG systems [37]. Badra [32] investigated SF and SA systems and modeled the equilibrium data to the Cohn equation, obtaining $K_s$ values of the same order of magnitude. The author used the same SA at different pHs and found that the increase in pH did not cause significant effects on the salting-out phenomenon. In addition to the difference in the proportion of M and G groups, the SAs used differ significantly in relation to their viscosity and molar mass, which are higher in G-alginate. It is possible that, as it has a longer chain, alginate-G has a greater molar volume, requiring more water molecules to solvate it, and, therefore, the salting out effect is more pronounced when alginate-G is used in the SF/SA blend.

## 5. Conclusion

It was possible to identify differences between the compositions of the SAs used. The proportion between M and G groups has a significant influence on the thermodynamic equilibrium of SF and SA blends. By using the equilibrium data, the phase diagram data were fitted to thermodynamic models of Flory–Huggins, NRTL, and UNIQUAC, in addition to verifying the salting-out effect of each SA from the Cohn equation. The thermodynamic model that presented the best fit to the equilibrium experimental data was UNIQUAC, presenting the lowest mean square deviation value. For NRTL and UNIQUAC models, it was possible to observe differences in the interaction parameters between the systems that used alginate-M and alginate-G, indicating that these thermodynamic models were more sensitive to variations in the SAs used in each system. Regarding the solubility parameters, alginate-G showed a higher constant value of $K_s$, being more efficient in precipitating SF.

These results represent an advance in the thermodynamic study of blends using SF and SA, natural polymers that have high potential for application as biomaterials. The results emphasize the importance of the source of natural polymers and the precise characterization of their composition, since these factors may have a significant influence on blend characteristics and, consequently, on blend final applications. It is expected that the data presented will be used as a basis and guide for further studies, aiming the application of fibroin and alginate in biomaterials or theoretical studies of the interaction of this protein with other macromolecules.

## Data Availability

No data are used in this study.

## Additional Points

*Highlights*. Influence of sodium alginate mannuronic and guluronic groups on the interaction with silk fibroin. Thermodynamic modeling of silk fibroin and sodium alginate blends using Flory–Huggins, NRTL, and UNIQUAC models. Use of the Cohn equation to analyze the potential of sodium alginate to precipitate the silk fibroin in solution.

## Conflicts of Interest

The authors declare that they have no known competing financial interests or personal relationships that could have appeared to influence the work reported in this paper.

## Acknowledgments

The authors acknowledge the financial support of the Coordenação de Aperfeiçoamento de Pessoal de Nível Superior—Brazil (CAPES)—Finance Code 001.

## Supplementary Materials

Figure S1: graphical abstract illustrating a silk fibroin and sodium alginate blend after phase separation in liquid and solid phases. Figure S2: hydrogen RMN spectra ($^1$H-RMN) for alginate-M (a) and alginate-G (b) using $D_2O$ as solvent at 70°C. Table S1: average of molar fraction ($n = 3$) of silk fibroin (SF), sodium alginate (alginate-M and alginate-G), and water in liquid and solid phases. Table S2: values of mass fraction for silk fibroin, alginate-M, and water calculated with Flory–Huggins model. Table S3: values of mass fraction for silk fibroin, alginate-G, and water calculated with Flory–Huggins model. Table S4: values of mass fraction for silk fibroin, alginate-M, and water calculated with NRTL model. Table S5: values of mass fraction for silk fibroin, alginate-G, and water calculated with NRTL model. Table

S6: values of mass fraction for silk fibroin, alginate-M, and water calculated with UNIQUAC model. Table S7: values of mass fraction for silk fibroin, alginate-G, and water calculated with UNIQUAC model. (*Supplementary Materials*)

## References


[1] B. Kundu, R. Rajkhowa, S. C. Kundu, and X. Wang, "Silk fibroin biomaterials for tissue regenerations," *Advanced Drug Delivery Reviews*, vol. 65, no. 4, pp. 457–470, 2013.

[2] E. Onsøyen, "Alginates," in *Thickening and Gelling Agents for Food*, A. P. Imeson, Ed., pp. 22–44, Springer, Boston, MA, 1997.

[3] A. Verma, S. Thakur, G. Mamba et al., "Graphite modified sodium alginate hydrogel composite for efficient removal of malachite green dye," *International Journal of Biological Macromolecules*, vol. 148, pp. 1130–1139, 2020.

[4] S. Thakur, B. Sharma, A. Verma, J. Chaudhary, S. Tamulevicius, and V. K. Thakur, "Recent progress in sodium alginate based sustainable hydrogels for environmental applications," *Journal of Cleaner Production*, vol. 198, pp. 143–159, 2018.

[5] S. Thakur, A. Verma, V. Kumar et al., "Cellulosic biomass-based sustainable hydrogels for wastewater remediation: chemistry and prospective," *Fuel*, vol. 309, Article ID 122114, 2022.

[6] M. A. de Moraes, M. F. Silva, R. F. Weska, and M. M. Beppu, "Silk fibroin and sodium alginate blend: miscibility and physical characteristics," *Materials Science and Engineering: C*, vol. 40, pp. 85–91, 2014.

[7] Y. Srisuwan and Y. Baimark, "Preparation of biodegradable silk fibroin/alginate blend films for controlled release of antimicrobial drugs," *Advances in Materials Science and Engineering*, vol. 2013, Article ID 412458, 6 pages, 2013.

[8] L.-D. Koh, Y. Cheng, C.-P. Teng et al., "Structures, mechanical properties and applications of silk fibroin materials," *Progress in Polymer Science*, vol. 46, pp. 86–110, 2015.

[9] Y. Wang, S. Fan, Y. Li et al., "Silk fibroin/sodium alginate composite porous materials with controllable degradation," *International Journal of Biological Macromolecules*, vol. 165, pp. 1314–1322, 2020.

[10] L. M. Lopes, M. A. de Moraes, and M. M. Beppu, "Phase diagram and estimation of Flory–Huggins parameter of interaction of silk fibroin/sodium alginate blends," *Frontiers in Bioengineering and Biotechnology*, vol. 8, Article ID 973, 2020.

[11] L. M. Lopes, M. A. de Moraes, and M. M. Beppu, "Study of phase separation in blends of silk fibroin and sodium alginate in solution and in solid state," *Journal of Polymer Research*, vol. 25, no. 9, 2018.

[12] Y. Wang, X. Wang, J. Shi et al., "A biomimetic silk fibroin/sodium alginate composite scaffold for soft tissue engineering," *Scientific Reports*, vol. 6, no. 1, Article ID 39477, 2016.

[13] J. Ming and B. Zuo, "A novel silk fibroin/sodium alginate hybrid scaffolds," *Polymer Engineering & Science*, vol. 54, no. 1, pp. 129–136, 2014.

[14] J. Ming and B. Zuo, "Crystal growth of calcium carbonate in silk fibroin/sodium alginate hydrogel," *Journal of Crystal Growth*, vol. 386, pp. 154–161, 2014.

[15] M. A. de Moraes and M. M. Beppu, "Biocomposite membranes of sodium alginate and silk fibroin fibers for biomedical applications," *Journal of Applied Polymer Science*, vol. 130, no. 5, pp. 3451–3457, 2013.

[16] K. I. Draget, G. Skjåk Bræk, and O. Smidsrød, "Alginic acid gels: the effect of alginate chemical composition and molecular weight," *Carbohydrate Polymers*, vol. 25, no. 1, pp. 31–38, 1994.

[17] C. X. Liang and K. Hirabayashi, "Improvements of the physical properties of fibroin membranes with sodium alginate," *Journal of Applied Polymer Science*, vol. 45, no. 11, pp. 1937–1943, 1992.

[18] Z. Wang, H. Yang, and Z. Zhu, "Study on the blends of silk fibroin and sodium alginate: hydrogen bond formation, structure and properties," *Polymer*, vol. 163, pp. 144–153, 2019.

[19] L. Lopes, M. A. de Moraes, and M. M. Beppu, "The phase equilibrium and thermodynamic modeling for silk fibroin and sodium alginate blends with different proportion of guluronic and mannuronic groups," *SSRN Electronic Journal*, 2022.

[20] S. Sohn, H. H. Strey, and S. P. Gido, "Phase behavior and hydration of silk fibroin," *Biomacromolecules*, vol. 5, no. 3, pp. 751–757, 2004.

[21] H. Grasdalen, "High-field, 1H-n.m.r. spectroscopy of alginate: sequential structure and linkage conformations," *Carbohydrate Research*, vol. 118, pp. 255–260, 1983.

[22] K. Y. Lee, J. A. Rowley, P. Eiselt, E. M. Moy, K. H. Bouhadir, and D. J. Mooney, "Controlling mechanical and swelling properties of alginate hydrogels independently by cross-linker type and cross-linking density," *Macromolecules*, vol. 33, no. 11, pp. 4291–4294, 2000.

[23] N. Minoura, M. Tsukada, and M. Nagura, "Fine structure and oxygen permeability of silk fibroin membrane treated with methanol," *Polymer*, vol. 31, no. 2, pp. 265–269, 1990.

[24] L. Stragevitch, *Equilíbrio Líquido-Líquido de Misturas de Não Eletrólitos*, Universidade Estadual de Campinas, 1997.

[25] M. M. Smith, J. M. Van-Ness, and G. C. Abbott, *Introdução à Termodinâmica da Engenharia Química, 7o edição LTC*, Rio de Janieor, 2007.

[26] E. J. Cohn, "The physical chemistry of the proteins," *Physiological Reviews*, vol. 5, no. 3, pp. 349–437, 1925.

[27] G. P. Parchen, *Efeito do Potencial Elétrico da Superfície de Lipossomas Revestidos Com Biopolímeros Sobre a Liberação Cutânea de EGF*, Universidade Federal do Paraná, 2001.

[28] K. I. Draget, G. Skjåk-Bræk, and O. Smidsrød, "Alginate based new materials," *International Journal of Biological Macromolecules*, vol. 21, no. 1-2, pp. 47–55, 1997.

[29] C. Sartori, D. S. Finch, B. Ralph, and K. Gilding, "Determination of the cation content of alginate thin films by FTi.r. spectroscopy," *Polymer*, vol. 38, no. 1, pp. 43–51, 1997.

[30] Y. A. Antonov and P. Moldenaers, "Structure formation and phase-separation behaviour of aqueous casein-alginate emulsions in the presence of strong polyelectrolyte," *Food Hydrocolloids*, vol. 25, no. 3, pp. 350–360, 2011.

[31] J.-L. Mession, A. Assifaoui, C. Lafarge, R. Saurel, and P. Cayot, "Protein aggregation induced by phase separation in a pea proteins–sodium alginate–water ternary system," *Food Hydrocolloids*, vol. 28, no. 2, pp. 333–343, 2012.

[32] S. B. Badra, *Estudo do Equilíbrio de Fases em Sistemas Contendo Polímeros Naturais: Fibroína de Seda e Alginato de Sódio*, Universidade de São Paulo, 2019.

[33] X. Li, Y. Hua, A. Qiu, C. Yang, and S. Cui, "Phase behavior and microstructure of preheated soy proteins and $\kappa$-carrageenan mixtures," *Food Hydrocolloids*, vol. 22, no. 5, pp. 845–853, 2008.

[34] A. W. Chan and R. J. Neufeld, "Modeling the controllable pH-responsive swelling and pore size of networked alginate based

biomaterials," *Biomaterials*, vol. 30, no. 30, pp. 6119–6129, 2009.

[35] J. L. Whittaker, N. R. Choudhury, N. K. Dutta, and A. Zannettino, "Facile and rapid ruthenium mediated photocrosslinking of *Bombyx mori* silk fibroin," *Journal of Materials Chemistry B*, vol. 2, no. 37, pp. 6259–6270, 2014.

[36] S. N. Timasheff, "The control of protein stability and association by weak interactions with water: how do solvents affect these processes?" *Annual Review of Biophysics and Biomolecular Structure*, vol. 22, no. 1, pp. 67–97, 1993.

[37] A. Matsumoto, J. Chen, A. L. Collette et al., "Mechanisms of silk fibroin sol−gel transitions," *The Journal of Physical Chemistry B*, vol. 110, no. 43, pp. 21630–21638, 2006.